Klein tunneling in binary photonic superlattices

S. Longhi
Dipartimento di Fisica, Politecnico di Milano, Piazza L. da Vinci 32, I-20133 Milano, Italy
(Received 17 November 2009; revised manuscript received 28 December 2009; published 2 February 2010)

A photonic analog of Klein tunneling for a relativistic electron across a potential step, based on spatial light propagation in an engineered binary waveguide array, is proposed. Klein tunneling can be simply visualized as optical beam refraction through a step-index interface, superimposed to the superlattice, and explained as an interband tunneling process between positive-energy (electron) and negative-energy (positron) minibands of the superlattice. Inhibition of Klein tunneling for a smooth potential step is also demonstrated.

DOI: 10.1103/PhysRevB.81.075102 PACS number(s): 78.67.Pt, 03.65.Xp, 42.79.Gn

I. INTRODUCTION

Klein tunneling (KT) refers to the prediction that relativistic fermions can pass through large repulsive potential steps without the exponential damping expected in quantum tunneling processes of nonrelativistic particles.[1,2] This phenomenon is a property of relativistic wave equations and arises from the existence of negative-energy solutions of the Dirac equation (see, for instance, Refs. 3 and 4 and references therein). KT for relativistic electrons, however, has never been observed. Its experimental observation would require extremely high fields which are not currently available. Additionally, as shown by Sauter,[5] KT is observable provided that the potential step is so steep to occur at distances comparable or smaller than the Compton wavelength: the probability of KT for a particle in a smoothly varying potential step, in fact, is greatly reduced and the step becomes basically impenetrable as in nonrelativistic tunneling theory. As KT has been for long time regarded as a relativistic effect rooted in the Dirac equation and associated to particle-antiparticle pairs creation, several authors have recently shown that it is a generic feature of wave-packet dynamics in spinor systems with certain linear dispersion relations, and can thus occur also for nonrelativistic particles. In particular, charge carriers in monolayer graphene behave as massless Dirac fermions which can undergo KT (see, for instance, Refs. 6–11 and reference therein). Experimental evidences of KT have been reported very recently in graphene[12,13] and in carbon nanotubes.[14] Photonic analogs of Dirac equation have been also theoretically proposed for light propagation in certain triangular or honeycomb photonic crystals. Similarly to graphene, the energy bands in such crystals may show a conical singularity, around which field propagation is described by a two-dimensional Dirac equation for a relativistic massless particle.[15–20] Following such a similarity, photonic analogs of relativistic phenomena for massless Dirac fermions in two-dimensional photonic crystals, including Zitterbewegung[19] and KT,[21] have been recently proposed. A photonic analog of KT has been also suggested exploiting negative refraction in metamaterials.[22]

In this work a different photonic analog of KT, based on spatial light propagation in a one-dimensional binary photonic superlattice,[23] is theoretically proposed. As compared to previous photonic analogs of KT based on two-dimensional honeycomb or triangular photonic crystals[16,19,21] or on metamaterials,[22] the present proposal offers an easier realization and enables a simple visualization in space of wave-packet dynamics in a KT process,[4] which is currently inaccessible in graphene systems.

II. BEAM PROPAGATION IN A BINARY SUPERLATTICE AND QUANTUM-OPTICAL ANALOGY

A. Model

The starting point of our analysis is provided by a rather standard model describing light transport in a one-dimensional binary photonic superlattice realized by two interleaved lattices A and B, as shown in Fig. 1(a). In practice,

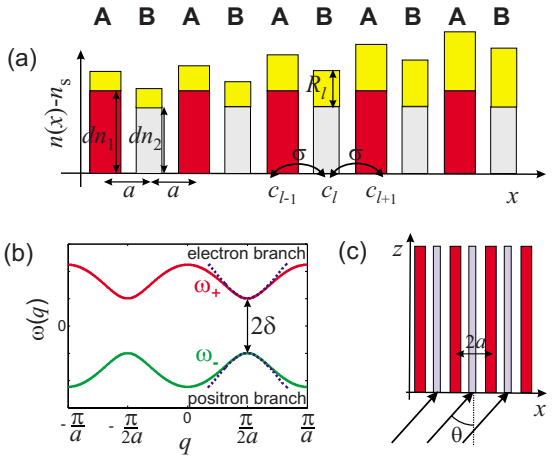

FIG. 1. (Color online) (a) Schematic of a binary superlattice, made of two interleaved lattices A and B of waveguides with high (dn_1) and low (dn_2) refractive index changes, equally spaced by a. Note that the period of the superlattice is $2a$. A modulation of refractive index depth R_l, superimposed to the two lattices A and B that mimics an external scalar potential in the Dirac Eq. (4), is also shown. Note that the superimposed index change is the same for waveguides of sublattices A and B belonging to the same dimer, i.e., $R_{2l-1}=R_{2l}$, which implies $\Phi_{2l-1}=\Phi_{2l}$ in Eq. (2). (b) Dispersion curves (minibands) of the tight-binding binary superlattice [Eq. (3)] for $\Phi=0$ (solid curves) and corresponding electron and positron dispersion curves of the Dirac Eq. (4) near the Brillouin zone edge $q=\pi/(2a)$ (dotted curves). (c) Broad beam excitation geometry of the binary superlattice. The tilt angle θ of the input beam is close to the Bragg angle θ_B.

the superlattice is realized by a sequence of equally spaced waveguides with alternating deep/shallow peak refractive index changes dn_1 and dn_2, and with a normalized waveguide index profile $h(x)$ that is assumed to be the same for the two lattices A and B.[23] A weak modulation R_l of the index change, much smaller than either dn_1 and dn_2 and equal for the interleaved lattices A and B, i.e., such that $R_{2l-1}=R_{2l}$, is also superimposed as shown in Fig. 1(a). The refractive index profile $n(x)$ of the superlattice can be thus written as $n(x)=n_s+\Sigma_l(dn_1+R_{2l})h(x-2la)+\Sigma_l(dn_2+R_{2l})h(x-2la+a)$, where a is the waveguide spacing and n_s the substrate refractive index. Propagation of monochromatic light waves at wavelength λ is described by the scalar wave equation (see, for instance, Ref. 24)

$$i\frac{\partial E}{\partial z}=-\frac{\lambda}{4\pi n_s}\frac{\partial^2 E}{\partial x^2}+2\pi\frac{n_s-n(x)}{\lambda}E, \tag{1}$$

which is valid in the paraxial and weak guidance approximations. In the tight-binding limit, light transport in the lattice can be described by means of coupled-mode equations for the fundamental-mode field amplitudes c_l in the various waveguides (see, for instance, Refs. 23, 25, and 26)

$$i(dc_l/dz)=-\sigma(c_{l+1}+c_{l-1})+(-1)^l\delta c_l+\Phi_l c_l, \tag{2}$$

where 2δ and σ are the propagation constant mismatch and the coupling rate between two adjacent waveguides of lattices A and B. The weak modulation R_l of the refractive index change is responsible, at leading order, to a slight change Φ_l of the modal propagation constants in the various waveguides, which is accounted for by the last term on the right-hand side of Eq. (2). Note that, for an index change R_l uniform in the various waveguides, i.e., for $\Phi_l=\Phi$ independent of index l, the tight-binding model (2) supports two minibands, whose dispersion curves are readily calculated by making the plane-wave Ansatz $c_l(q)\sim\exp(iqla-i\omega z)$ and read[25]

$$\omega_{\pm}(q,\Phi)=\Phi\pm\sqrt{\delta^2+4\sigma^2\cos^2(qa)} \tag{3}$$

[see Fig. 1(b)]. It should be noted that the tight-binding model (2) is accurate to describe beam dynamics of Eq. (1) provided that the first two minibands of the array are mainly excited at the input plane. Such a condition is usually satisfied provided that the width of angular spectrum of the beam profile $E(x,0)$ at the input plane does not exceed a characteristic angle $\theta_L\sim\beta\theta_B$, where $\theta_B=\lambda/(4n_sa)$ is the Bragg angle and β is of order ~ 1 (see, for instance, Refs. 26–28). At higher excitation angles, higher-order bands may enter into the dynamics (see the discussion in Sec. IV below), however they do not play any role in the KT process and the analogy between photonic and relativistic KT can be thus established within the tight-binding model (2).

B. Quantum-optical analogy

In this section we outline the quantum-optical analogy between KT of relativistic massive fermions across a potential step and beam dynamics in a binary superlattice described by the tight-binding model (2). In Ref. 29, it was recently shown that, near the Brillouin zone edge $q=\pm\pi/(2a)$, the dispersion relations (3) of a uniform superlattice approximate the positive (electron) and negative (positron) energy curves of a massive Dirac electron, and that propagation of broad beams tilted at the Bragg angle $\theta_B=\lambda/(4n_sa)$ mimics the temporal dynamics of the relativistic free Dirac electron. To study the photonic analog of KT in a binary superlattice, we extend the analysis of Ref. 29 to include the effects of the superimposed modulation Φ_l of propagation constants. As it will be shown below, such a modulation mimics an external scalar (electrostatic-type) potential in the Dirac equation. Let us assume that the array is excited by a broad beam (e.g., Gaussian shaped) incident onto the array at an angle close to the Bragg angle, i.e., $E(x,0)=G(x)\exp(2\pi i\theta_B n_s x/\lambda)$, where $G(x)$ varies slowly on the spatial scale $\sim a$ [see Fig. 1(c)].[30] At such an incidence angle, the modes in adjacent waveguides are thus excited with a nearly equal amplitude but with a phase difference of $\pi/2$. After setting $c_{2l}(z)=(-1)^l\psi_1(l,z)$, $c_{2l-1}=-i(-1)^l\psi_2(l,z)$, and assuming that Φ_l varies slowly with l, the amplitudes ψ_1 and ψ_2 vary slowly with l, and one can thus write $\psi_{1,2}(l\pm 1,z)=\psi_{1,2}(l,z)\pm(\partial\psi_{1,2}/\partial l)$ and consider $l\equiv\xi=x/(2a)$ as a continuous variable rather than as an integer index. Under such assumptions from Eq. (2) it readily follows that the two-component spinor $\psi(\xi,z)=(\psi_1,\psi_2)^T$ satisfies the one-dimensional Dirac equation in presence of an external electrostatic potential

$$i\frac{\partial\psi}{\partial z}-\Phi(\xi)\psi+i\sigma\alpha\frac{\partial\psi}{\partial\xi}-\delta\beta\psi=0, \tag{4}$$

where

$$\alpha=\begin{pmatrix}0 & 1\\ 1 & 0\end{pmatrix},\quad \beta=\begin{pmatrix}1 & 0\\ 0 & -1\end{pmatrix}, \tag{5}$$

are the σ_x and σ_z Pauli matrices, respectively, and $\Phi(\xi)=\Phi_{2l}=\Phi_{2l-1}$. Note that, after the formal change $\sigma\to c$, $\delta\to mc^2/\hbar$, $\xi\to x$, $\Phi\to V/\hbar$, and $z\to t$, Eq. (4) corresponds to the one-dimensional Dirac equation for an electron of mass m in presence of the scalar potential $V(x)$ (see, for instance, Ref. 2). Note also that, in our optical analog, the *temporal* evolution of the spinor wave function ψ for the Dirac electron is mapped into the *spatial* evolution of the field amplitudes ψ_1 and ψ_2 along the z axis of the array, and that the two components ψ_1, ψ_2 of the spinor wave function correspond to the occupation amplitudes in the two sublattices A and B composing the superlattice. For a uniform potential, the energy-momentum dispersion relation $\hbar\omega(k)$ of the Dirac Eq. (4), obtained by making the Ansatz $\psi\sim\exp(ik\xi-i\omega z)$ in Eq. (4), is composed by the two branches $\omega_{\pm}(k)=\Phi\pm\epsilon(k)$, corresponding to positive- and negative-energy states of the relativistic free electron, where

$$\epsilon(k)=\sqrt{\delta^2+\sigma^2k^2}. \tag{6}$$

Note that such two branch curves are readily obtained from Eq. (3) after setting $q\to\pi/(2a)+k/(2a)$ and assuming small values of k, i.e., they approximate the exact dispersion curves of the two minibands of the binary array near the boundary of the Brillouin zone [see Fig. 1(b)].

III. KLEIN TUNNELING

Let us consider now a potential step, $\Phi=0$ for $\xi<0$ and $\Phi=\Phi_0>0$ for $\xi>0$, and assume that at the input plane $z=0$ the wave-packet $\psi(\xi,0)$ is localized in the $\xi<0$ region, far from the step, with a spectrum peaked at around $k=k_0>0$. Note that, for the excitation geometry shown in Fig. 1(c), at the input plane one has $\psi_1(\xi,0)\propto G(2la)$ and $\psi_2(\xi,0)\propto G(2la-a)$. The positive- and negative-energy components of the wave-packet split during propagation, with the positive (electron) energy component wave packet that propagates toward the potential step at $\xi=0$ and the negative (positron) energy component moving in the opposite direction (see Figs. 5 and 6 to be commented below). In the optical language, this splitting is caused by the different refraction angles of the beams belonging to the two minibands of the array (see, for instance, Ref. 26). The regime of KT, corresponding to the positive-energy wave packet passing through the large repulsive step without exponential damping, is attained when the energy of the incident wave packet falls inside the negative (positron) energy branch at $\xi>0$, i.e., when $\Phi_0>\delta+\omega_0$, where $\omega_0=\sqrt{\delta^2+k_0^2\sigma^2}$ (see, for instance, Ref. 4). We refer to this case as the Klein region, or "region II." Conversely, for $\Phi_0<\delta+\omega_0$ and in the classically forbidden region $\Phi_0>\omega_0-\delta$ (region I or nonrelativistic tunneling regime), the wave packet does not propagate in the $\xi>0$ region, and an evanescent field occurs in such a region like for the problem of tunneling of a nonrelativistic particle. Such behaviors are illustrated in Fig. 2. In the optical context, KT can be simply viewed as an interband tunneling process between the second and the first mininbands of the binary array, at the two sides $\xi<0$ and $\xi>0$ of the step, which are partially overlapped owing to the applied refractive index step Φ_0 [see the lower plot in Fig. 2(b) or the right plot in Fig. 3(c), to be discussed later]. It should be noted that, as opposed to a similar interband tunneling process that one could observe at the interface between two different and suitably engineered singly periodic arrays (see, for instance, Ref. 31), a correct analogy with KT of massive relativistic electrons can be established when dealing with a binary superlattice structure. In fact, as already noticed for graphene systems,[8] the similarity between photonic and relativistic KT requires more than the similarity of certain dispersion relations for two bands or their partial overlap at the interface enabling the observation of a tunneling (refraction) process. What is important in the Dirac Eq. (4) is the interconnection between the spinor wave function components ψ_1 and ψ_2, which in our superlattice structure are represented by the occupation amplitudes of the two sublattices A and B. Such interconnection would be lost in case of an interface of two

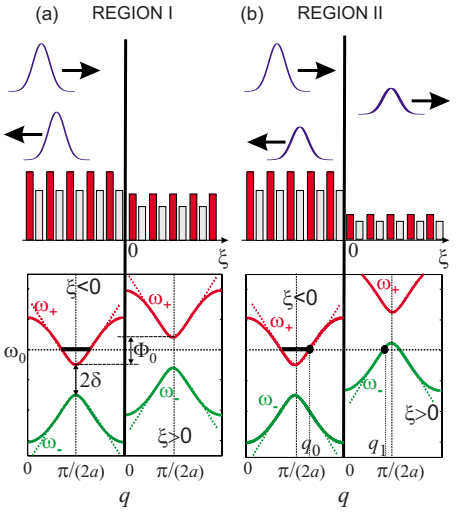

FIG. 2. (Color online) Schematic of two different tunneling regimes (regions I and II) in a binary superlattice with a step potential Φ_0 corresponding to (a) the nonrelativistic regime (the potential step is impenetrable and an incident wave packet is totally reflected) and (b) the relativistic KT region at an increased value of Φ_0.

different singly periodic lattices with well-separated bands. In such systems, beam dynamics at the top or at the bottom of two different bands, overlapped at the interface as in Fig. 2(b), would be described more naturally by two *independent* Schrödinger-like equations, with different and of opposite sign for the effective masses, rather than by a Dirac equation for a spinor wave function. It should be also noticed that, as compared to the problem of KT for a relativistic electron,[2–4] in our optical analog the power transmission T and reflection R coefficients of a wave packet incident onto the potential step always satisfy the power conservation law $R+T=1$, and the phenomenon of electron-positron pairs creation at the potential step, encountered in the context of the hole theory of KT and leading to the somewhat paradoxical result $R>1$, does not occur in our classical analog.[32]

The calculation of the transmission coefficient T can be done analytically within the coupled-mode equation model (2) by looking for plane-wave solutions as a superposition of incident, reflected, and transmitted waves after appropriate boundary conditions are applied at the interface. Denoting by $q_0=\pi/(2a)+k_0/(2a)$ (with $0<k_0<\pi$ to ensure a positive group velocity) the wave number of the incident wave (belonging to the upper miniband ω_+ of the binary array) and by q_1 the wave number of the transmitted wave (belonging to the lower miniband ω_- of the array), the following expression for power transmission T is obtained in the Klein region [region II of Fig. 2(b)]

$$T=\frac{(\omega_0-\delta)(\omega_0-\delta-\Phi_0)\sin(2q_0a)\sin(2q_1a)}{[\Phi_0\cos(q_0a)\cos(q_1a)]^2+[(\omega_0-\delta)\sin(q_0a)\cos(q_1a)+(\omega_0-\delta-\Phi_0)\sin(q_1a)\cos(q_0a)]^2}, \tag{7}$$

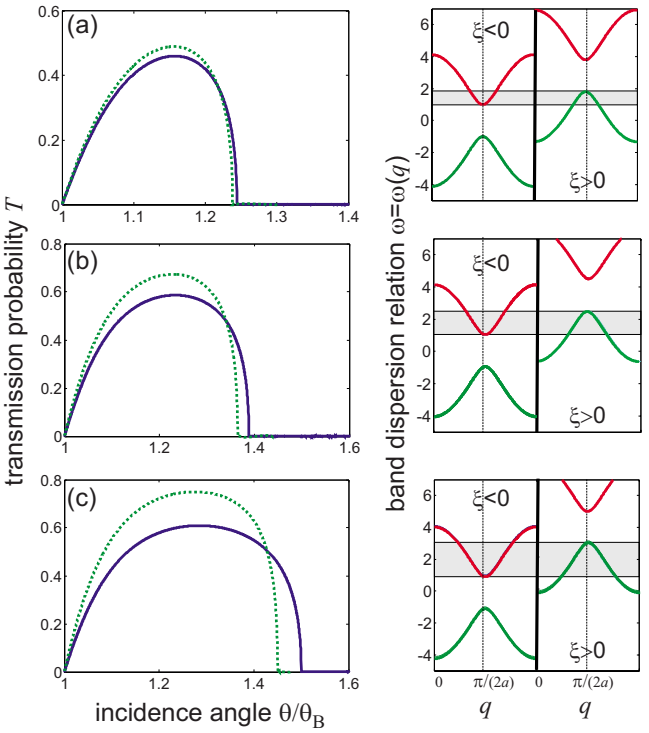

FIG. 3. (Color online) Behavior of power transmission coefficient T (solid curves) in a binary superlattice with a potential step, as predicted by Eq. (7), versus the incidence angle θ, normalized to the Bragg angle θ_B, for $\sigma=2$, $\delta=1$, and for increasing values of the potential step Φ_0: (a) $\Phi_0=2.8$, (b) $\Phi_0=3.5$, and (c) $\Phi_0=4$. The dotted curves show, for comparison, the behavior of power transmission T_D for KT as predicted by the Dirac Eq. (4) [see Eq. (A18) in the Appendix]. The pictures on the right show the corresponding band diagrams of the tight-binding superlattice in the $\xi<0$ and $\xi>0$ regions. The overlapping between lower (positron) and upper (electron) minibands, necessary to achieve KT, are evidenced by the shaded regions. The upper and lower limits of the overlapping regions define the cut-off angles of nonvanishing transmission in the T curves of left panels.

where $\omega_0=\omega_+(q_0,0)$ and $\omega_+(q,\Phi)$ is defined by Eq. (3). The derivation of Eq. (7) is detailed in the Appendix. The wave number q_1 of transmitted wave is obtained from the energy conservation condition

$$\omega_-(q_1,\Phi_0)=\omega_+(q_0,0), \tag{8}$$

with the constrain $0<q_1<\pi/(2a)$ to ensure a positive group velocity of the transmitted wave packet (see the Appendix). A simple geometric determination of q_1 in region II is depicted in Fig. 2(b). A typical behavior of the transmission coefficient T, versus the incidence angle θ, normalized to the Bragg angle θ_B, is shown in Fig. 3 for a few values of step height Φ_0. Note that the wave number q_0 entering in Eq. (7) is related to the incidence angle θ by the simple relation

$$q_0=\frac{\pi}{2a}\frac{\theta}{\theta_B}. \tag{9}$$

In the figure, the transmission coefficient T_D, as predicted for KT in the framework of the Dirac Eq. (4), is shown for comparison by the dotted curves (see the Appendix for the explicit expression of T_D). Note that, as expected, the two curves T and T_D well overlap provided that the energy state involved in the tunneling process belongs to the bottom of the upper miniband at $\xi<0$ (positive energy or electron branch) and to the top of the lower miniband at $\xi>0$ (negative energy or positron branch), as in Fig. 3(a). In this case, in fact, the discrete model (2) can be safely approximated by the continuous Dirac Eq. (4) along the lines detailed in Sec. II B.

IV. NUMERICAL RESULTS

We checked the correctness of the theoretical analysis, based on the tight-binding model (2), and the feasibility of an experimental observation of a photonic analog of KT in binary superlattices by direct numerical simulations of the paraxial wave Eq. (1) based on a standard pseudospectral split-step beam propagation method. Parameter values and refractive index profiles used in the simulations typically apply to binary arrays realized in fused silica by femtosecond laser writing and excited in the visible at $\lambda=633$ nm.[23] Figure 4(a) shows the index profile $n(x)$ of the uniform superlattice (i.e., with $R_l=0$) used in the simulations, corresponding to a waveguide spacing $a=10$ μm, refractive index changes $dn_1=0.002$ and $dn_2=0.00196$, and a substrate refractive index $n_s=1.42$. The Bragg angle at $\lambda=633$ nm is thus $\theta_B\simeq 0.64°$. Figure 4(b) shows the corresponding dispersion curves $\omega_n(q)$ of a few low-order bands of the superlattice (band diagram), normalized to $2\pi/\lambda$, numerically computed by a standard plane-wave expansion method. Note that the two lowest bands $n=1$ and $n=2$ in Fig. 4(b) correspond to the two minibands ω_- and ω_+, respectively, of the tight-

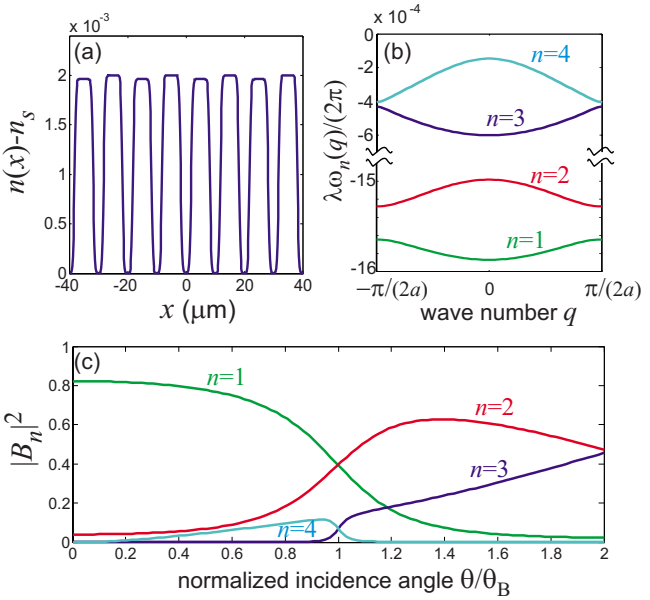

FIG. 4. (Color online) (a) Refractive index profile of the uniform binary superlattice used in numerical simulations, (b) corresponding band diagram, and (c) plane-wave excitation coefficients of the array versus incidence angle θ, normalized to the Bragg angle θ_B. Parameter values are given in the text.

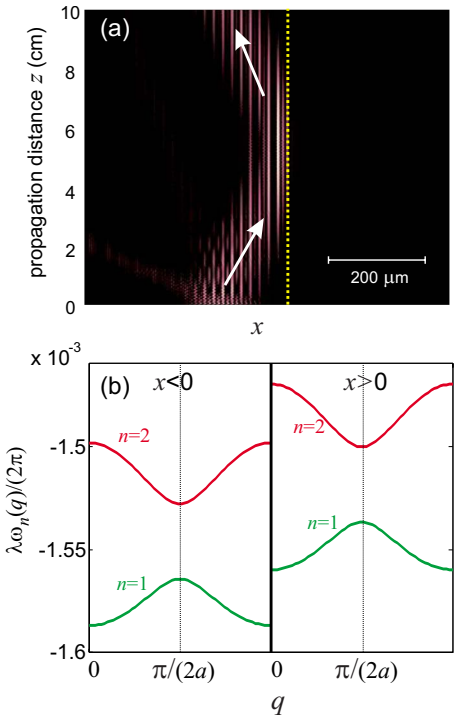

FIG. 5. (Color online) (a) Evolution of beam intensity (snapshot of $|E(x,z)|^2$) in the binary superlattice of Fig. 4 with a superimposed refractive index step $R=-3\times10^{-5}$ at $x=0$ and (b) corresponding band diagrams (lowest two minibands $n=1$ and $n=2$). The arrows in (a) indicate the incident and reflected beams, belonging to the $n=2$ miniband, whereas the vertical dotted line shows the position $x=0$ of the refractive index step. Note that total reflection at the interface occurs because the minibands $n=2$ at $x<0$ (electron energy branch) and $n=1$ at $x>0$ (positron energy band) are not overlapped [region I of Fig. 2(a)].

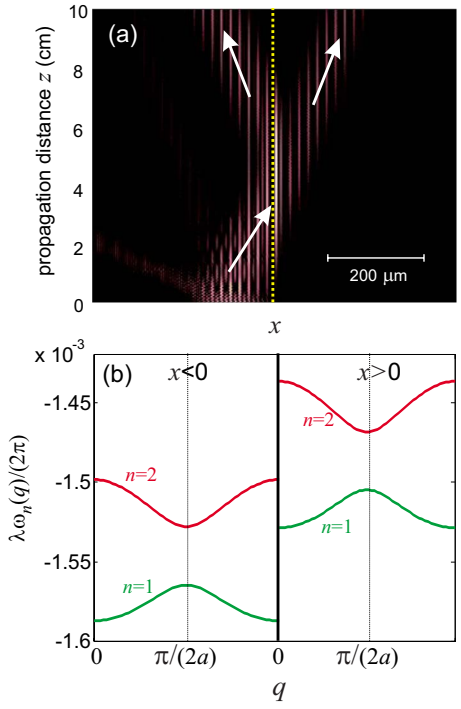

FIG. 6. (Color online) Same as Fig. 5, but for an increased refractive index step $R=-6.5\times10^{-5}$ corresponding to the KT region of Fig. 2(b). The arrows in (a) indicate the incident, reflected, and transmitted beams. Note that, as the incident and reflected beams belong the $n=2$ miniband (electron energy branch), the transmitted beam belongs to the $n=1$ miniband (positron energy branch).

binding model (2) depicted in Figs. 1(b), 2, and 3, which are involved in the KT process. Figure 4(c) shows the behavior of band excitation coefficients $|B_n|^2$ versus incidence angle θ for the few low-order bands of the superlattice. The Bloch-wave excitation coefficients $B_n(\theta)$ provide the weight of excited Bloch modes at different bands under plane-wave excitation of the array at tilting angle θ (for a formal definition and method of calculation of B_n we refer the reader to Refs. 26–28). Figures 5 and 6 show two examples of wave-packet tunneling in a 10-cm-long binary superlattice with a superimposed refractive index step ($R_l=0$ for $l\leq0$ and $R_l=R=$const. for $l\geq1$) corresponding to region I (nonrelativistic regime, $R=-3\times10^{-5}$) and region II (relativistic KT regime, $R=-6.5\times10^{-5}$) of Fig. 2, respectively. The exciting field in the $x<0$ region is a broad Gaussian beam of spot size $w_0=50$ μm, tilted at the angle $\theta=1.4\theta_B\simeq0.90°$, i.e., $E(x,0)=\exp[-(x/w_0)^2]\exp(2\pi i n_s\theta x/\lambda)$. As can be seen from Figs. 5 and 6, the input beam breaks into the superposition of different beams (three beams are clearly visible), belonging to the various bands of the superlattice and that refract at different angles (see, for instance, Ref. 28). At the chosen excitation angle ($\theta=1.4\theta_B$), according to Fig. 4(c) the miniband $n=2$ is mainly excited at the input plane, and the corresponding beam propagates toward the interface at $x=0$. The other two wave packets, clearly visible in Figs. 5 and 6 and belonging to bands $n=1$ and 3, propagate in the opposite direction and are thus not involved in the KT process. In case of Fig. 5, the potential step at the interface is not strong enough to reach the KT region [see the band diagram of Fig. 5(b)], and the wave packet is completely reflected from the interface as one can clearly see from the intensity beam evolution along the array plotted in Fig. 5(a). Conversely, if the potential step height is increased such that the "positron" energy branch (i.e., miniband $n=1$) at $x>0$ overlaps with the "electron" energy branch (i.e., miniband $n=2$) at $x<0$, as in case of Fig. 6, a partial transmission of the wave packet across the interface is clearly observed, which is a signature of KT [see Fig. 6(a)].

Finally, it is worth mentioning that our optical superlattice structure can be designed to demonstrate the disappearance of KT in a smooth potential step. According to the original prediction by Sauter,[5] to observe KT the rise of the potential step from $\Phi=0$ to $\Phi=\Phi_0$ should occur over a spatial scale not greater than the Compton wavelength $\lambda_C=h/(mc)$ (see also Refs. 3 and 33). According to the quantum-optical analogy established in Sec. II B, in our superlattice system the Compton wavelength, in units of waveguide spacing a, is replaced by $\lambda_C\rightarrow2\pi\sigma/\delta$. From the band diagram of Fig. 4(b), one can estimate $\sigma/\delta\sim1.1$, yielding $\lambda_C\sim6.9$. As an example, Fig. 7 shows the evolution of beam intensity (snapshot of $|E(x,z)|^2$) in the same binary superlattice of Fig. 6, but with the potential step R_l smoothly varying from $R=0$ to $R=-6.5\times10^{-5}$ over a few lattice periods as indicated in the right plots of Fig. 7. Note that, as the transition of R_l from a

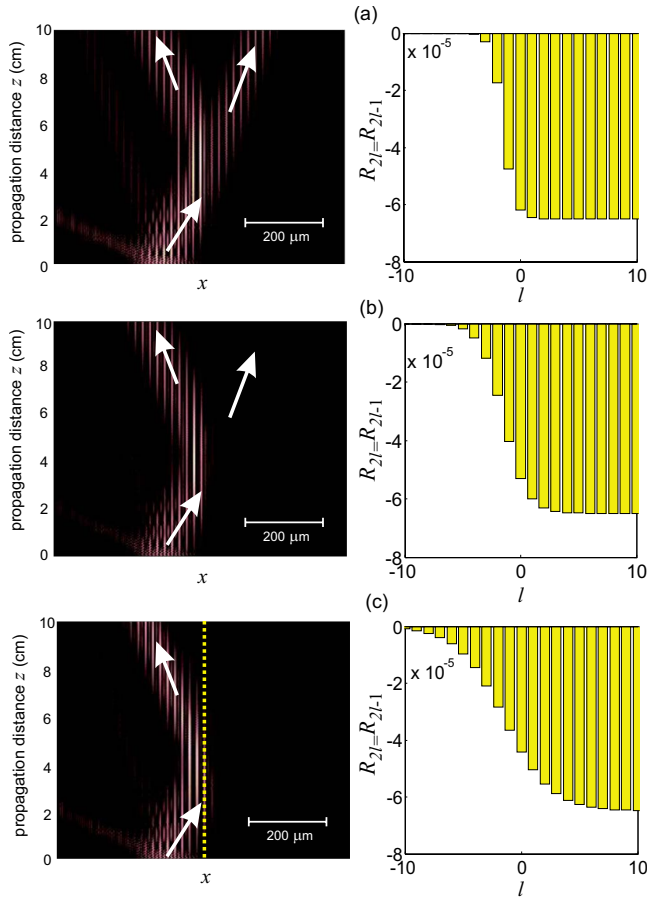

FIG. 7. (Color online) Same as Fig. 6, but for a smooth refractive index step, from $R_l=0$ at $l\to-\infty$ to $R_l=-6.5\times10^{-5}$ at $l\to\infty$, as indicated in the right plots. The transition from KT, for a steep change in refractive index [Fig. 7(a)], to inhibition of tunneling across the step, for a smoother change in refractive index [Figs. 7(b) and 7(c)], is clearly observed.

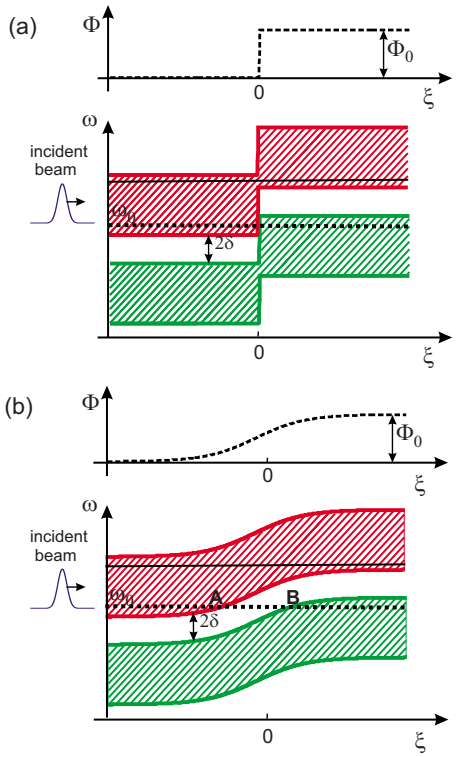

FIG. 8. (Color online) Band diagrams in the (ξ,ω) plane, showing the allowed energy intervals of the two minibands (electron and positron branches) versus spatial distance ξ, for (a) a sharp potential step and (b) a smooth potential step. The behavior of the potential $\Phi(\xi)$ is shown in the upper plots of (a) and (b).

low to a high potential gets smoother, beam transmission at the interface, corresponding to KT, is clearly inhibited [compare Figs. 7(a)–7(c)]. In the optical context, inhibition of light tunneling as the potential step gets smooth can be explained by considering the space-dependent band structure of the tight-binding superlattice, as shown in Fig. 8. The space-energy diagram represents, for a fixed value of position ξ, the allowed values of ω for propagative waves, which according to Eq. (3) are formed by two intervals separated by 2δ, each of width $(\sqrt{\delta^2+4\sigma^2}-\delta)$. Physically, the value of ω basically defines a correction to the propagation constant of the Bloch mode propagating in the lattice from the reference plane-wave value $2\pi n_s/\lambda$. As ξ varies along the lattice, the allowed values of ω describe the two areas represented by the shaded regions in Fig. 8, which define the analogous of the electron and positron energy branches. Such diagrams are similar to the energy band diagrams of a semiconductor, in which the two superlattice minibands play the role of the conduction and valence bands and the effect of the external potential $\Phi(\xi)$ is to curve the band structure. Let $\omega=\omega_0$ be the selected value of ω of the incident beam, and assume that the potential step height Φ_0 is large enough to be in the KT region of Fig. 2(b). As the beam propagates along the lattice, the value of ω is a constant of motion, and therefore it can be represented by an horizontal line in the band diagrams [the bold dotted horizontal curves in the lower plots of Figs. 8(a) and 8(b)]. As shown in Fig. 8(a), for a sharp potential step at the interface $\xi=0$ the electron and positron energy bands are overlapped, and the beam does not need to cross any forbidden region. However, owing to the sharp discontinuity of media properties, beam transmission is not complete, and some light is reflected like in a Fresnel discontinuity between two different dielectric media. Conversely, for a smooth potential step [see Fig. 8(b)] the beam has to cross a forbidden region, which behaves like a potential barrier. The width of the potential barrier is indicated by the segment AB in Fig. 8(b). Because the width AB increases as the potential step gets smoother, the corresponding tunneling probability, i.e., beam transmission across the interface, rapidly decreases. This explains the inhibition of KT observed in numerical simulations of Fig. 7. Finally, it is worth mentioning that the inhibition of light transmission for a smooth potential step is peculiar to the overlapping realized at $\omega=\omega_0$ between positive- and negative-energy minibands at $\xi<0$ and $\xi>0$. In fact, let us consider the case where the value ω_0, defined by the input beam launching condition, is increased such as to realize, at the interface $\xi=0$, an overlapping between the positive-energy bands. This condition is indicated by the horizontal thin solid line in Figs. 8(a) and 8(b). As one clearly sees from such figures, in this case for *both* a sharp [Fig. 8(a)] and a smooth [Fig. 8(b)] potential step the beam

does not need to cross any forbidden region, and thus beam transmission occurs also for a smooth potential. In this latter case, in the adiabatic approximation the transmission is even complete because the smooth change in the band properties avoids partial beam reflection due to the discontinuity of media properties.

V. CONCLUSIONS

In conclusion, a photonic analog of Klein tunneling for a relativistic electron across a potential step, based on spatial light propagation in a waveguide superlattice, has been proposed. In our optical analog, a correspondence between one-dimensional tunneling of the spinor wave function ψ for the Dirac electron and spatial beam evolution along the superlattice can be established, with the two components of ψ corresponding to the occupation amplitudes in the two sublattices composing the superlattice. Klein tunneling can be thus simply visualized as optical beam refraction through a step-index interface, superimposed to the superlattice, and explained as an interband tunneling process between positive-energy (electron) and negative-energy (positron) minibands of the superlattice. Design parameters to observe KT in binary superlattices with a sharp potential step, and inhibition of KT for a smooth potential step, have been proposed. In view of the excellent quality and control of waveguide arrays nowadays available by laser direct-writing methods[34] and owing to the possibility of a direct visualization of spatial light propagation by means of fluorescence microscopy techniques,[23,24] it is envisaged that the present results could motivate experimentalists toward the observation of a photonic analog of KT in one-dimensional optical superlattices. A possible extension of the present analysis could be the study of light transport and KT in two-dimensional superlattices, in which the larger dimensionality of the problem enables a richer engineering of the underlying Dirac-type Hamiltonian. For example, a two-dimensional array of straight waveguides arranged in a honeycomb lattice,[21] but with a propagation constant mismatch 2δ applied among waveguides in the two sublattices A and B of the honeycomb, could be designed to realize the analog of a two-dimensional massive Dirac particle. Unlike usual monolayer graphene-type systems describing massless Dirac fermions, for a nonvanishing value of δ the energy spectrum changes from the usual linear dispersion near the Dirac point to a hyperbolic dispersion due to the presence of an energy gap of the massive particle. When a superimposed index profile in applied to mimic an external potential, such honeycomb superlattices could be of interest to study the analog of two-dimensional tunneling of Dirac electrons through spatial regions of finite mass.[36]

APPENDIX: DERIVATION OF THE TRANSMISSION COEFFICIENT IN THE KLEIN TUNNELING REGION

In this Appendix we derive the expression of the transmission coefficient T [Eq. (7) given in the text] in a binary superlattice with a step potential in the region II (the KT region) schematically depicted in Fig. 2(b). To this aim, let us first note that, for a uniform potential $\Phi_l=\Phi$ (independent of index l), the plane-wave solutions (eigenstates) of coupled-mode Eqs. (2) corresponding to the wave number q are given by

$$c_l^{(+)}(q) = \begin{pmatrix} -2\sigma\cos(qa) \\ \omega_+ - \delta - \Phi \end{pmatrix} \exp(iqal - i\omega_+ z) \tag{A1}$$

for the positive-energy branch $\omega_+(q,\Phi)=\Phi+\sqrt{\delta^2+4\sigma^2\cos^2(qa)}$, and

$$c_l^{(-)}(q) = \begin{pmatrix} -2\sigma\cos(qa) \\ \omega_- - \delta - \Phi \end{pmatrix} \exp(iqal - i\omega_- z) \tag{A2}$$

for the negative-energy branch $\omega_-(q,\Phi)=\Phi-\sqrt{\delta^2+4\sigma^2\cos^2(qa)}$. In Eqs. (A1) and (A2), the upper (lower) row applies to an even (odd) value of index l. To construct the appropriate solution to Eqs. (2) corresponding to an incident, reflected, and transmitted wave packet in case of a potential step, it is worth noticing that, for q near $\pi/(2a)$, i.e., for q near the edge of the Brillouin zone, a wave packet belonging to the positive-energy branch, constructed by a superposition of plane waves according to Eq. (A1), propagates in the forward direction of the lattice for $q>\pi/(2a)$, and in the backward direction for $q<\pi/(2a)$, i.e., its group velocity $v_g=(d\omega_+/dq)$ is positive in the former case and negative in the latter case. The opposite holds for a wave packet belonging to the negative-energy branch, constructed by a superposition of plane waves according to Eq. (A2). Let us consider now a potential step by assuming $\Phi=0$ for $l\leq 0$ and $\Phi=\Phi_0$ for $l>0$, and let us consider an incident wave, belonging to the positive-energy branch ω_+ with wave number $q_0>\pi/(2a)$ that comes from $\xi\to-\infty$ and propagates toward the step. The step height Φ_0 is chosen such that to realize the KT region [region II of Fig. 2(b)]. In this case, there exists a real-valued wave number q_1, smaller than $\pi/(2a)$ such that [see also the lower plot of Fig. 2(b)]

$$\omega_-(\Phi_0,q_1) = \omega_+(0,q_0), \tag{A3}$$

i.e., the negative-energy eigenstate with wave number q_1 in the semiarray $\xi>0$ is in resonance with the positive-energy incoming state, of wave number q_0, at $\xi<0$. Note that a negative-energy wave packet with carrier wave number q_1 has a positive group velocity, i.e., it propagates in the forward direction far from the potential step, provided that $q_1<\pi/(2a)$. We can thus search for a stationary solution to Eq. (2) with a potential step in the form

$$c_l = \begin{cases} (a_l^{(i)} + r a_l^{(r)})\exp(-i\omega_0 z) & l \leq 1 \\ t a_l^{(t)} \exp(-i\omega_0 z) & l \geq 0 \end{cases}, \tag{A4}$$

where $\omega_0 \equiv \omega_+(0,q_0)=\omega_-(\Phi_0,q_1)$ and $a_l^{(i)}$, $a_l^{(r)}$, and $a_l^{(t)}$ are the incident, reflected, and transmitted propagative waves, respectively, defined by

$$a_l^{(i)} = \begin{pmatrix} -2\sigma\cos(q_0 a) \\ \omega_0 - \delta \end{pmatrix} \exp(iq_0 al), \tag{A5}$$

$$a_l^{(r)} = \begin{pmatrix} -2\sigma\cos(q_0 a) \\ \omega_0 - \delta \end{pmatrix} \exp(-iq_0 al), \tag{A6}$$

$$a_l^{(t)} = \begin{pmatrix} -2\sigma\cos(q_1 a) \\ \omega_0 - \delta - \Phi_0 \end{pmatrix} \exp(iq_1 al). \tag{A7}$$

In Eqs. (A5)–(A7), the upper (lower) rows apply to an even (odd) value of index l, whereas the complex coefficients r and t entering in Eqs. (A4) have to be determined by imposing the continuity of c_l at $l=0$ and $l=1$, i.e.,

$$ta_0^{(t)} = a_0^{(i)} + ra_0^{(r)}, \quad ta_1^{(t)} = a_1^{(i)} + ra_1^{(r)}. \tag{A8}$$

Substitution of Eqs. (A5)–(A7) into Eq. (A8) yields the following relations

$$\cos(q_1 a)t = (1+r)\cos(q_0 a), \tag{A9}$$

$$t\exp(iq_1 a) = \frac{(\omega_0 - \delta)[\exp(iq_0 a) + r\exp(-iq_0 a)]}{(\omega_0 - \delta - \Phi_0)}, \tag{A10}$$

which can be solved for r and t, obtaining

$$t = -\frac{i(\omega_0 - \delta)\sin(2q_0 a)}{(\omega_0 - \delta)\cos(q_1 a)\exp(-iq_0 a) - (\omega_0 - \delta - \Phi_0)\cos(q_0 a)\exp(iq_1 a)}, \tag{A11}$$

$$r = -\frac{2i(\omega_0 - \delta)\sin(q_0 a)\cos(q_1 a)}{(\omega_0 - \delta)\cos(q_1 a)\exp(-iq_0 a) - (\omega_0 - \delta - \Phi_0)\cos(q_0 a)\exp(iq_1 a)} - 1. \tag{A12}$$

Some care should be paid to correctly calculate the transmission and reflection coefficients T and R. Let us indicate by $J^{(i)}$, $J^{(r)}$, and $J^{(t)}$ the flux intensities associated to the incident, reflected, and transmitted waves, respectively. For the discrete Eq. (2), the appropriate definition of the intensity flux at site l is (see, for instance, Ref. 35)

$$J_l = i\sigma(c_l c_{l+1}^* - c_l^* c_{l+1}), \tag{A13}$$

and the discrete version of the continuity equation is $(d|c_l|^2/dz) + (J_l - J_{l-1}) = 0$. The correct definition of the power transmission and reflection coefficients, T and R, is thus

$$T = \left|\frac{J^{(t)}}{J^{(i)}}\right| \quad R = \left|\frac{J^{(r)}}{J^{(i)}}\right|, \tag{A14}$$

where the flux intensities $J^{(i)}$, $J^{(r)}$, and $J^{(t)}$ are calculated according to Eq. (A13). Using Eqs. (A5)–(A7), one then obtains

$$R = |r|^2, \quad T = |t|^2 \left|\frac{(\omega_0 - \delta - \Phi_0)\sin(2q_1 a)}{(\omega_0 - \delta)\sin(2q_0 a)}\right|. \tag{A15}$$

It can be readily shown from the previous equations that, according to power conservation, $R+T=1$. Substitution of Eq. (A11) into the Eq. (A15) finally yields Eq. (7) given in the text.

The determination of the power transmission coefficient in the framework of the Dirac Eq. (4), obtained as a continuous limit of the discrete model (2) under the assumptions discussed in the text, proceeds in a standard way which is detailed in many papers and textbooks (see, for instance, Refs. 2–4). For the sake of completeness, we just briefly give here the main results. Let $k_0 > 0$ be the wave number of an incident progressive plane wave on the positive-energy (electron) branch in the $\xi < 0$ region, which is related to the wave number q_0 previously introduced for the discrete model by the relation

$$q_0 = \frac{\pi}{2a} + \frac{k_0}{2a}. \tag{A16}$$

In the KT region, at $\xi > 0$ there exists a propagative (transmitted) wave belonging to the negative-energy (positron) branch which has the same energy as that of the incident wave. The wave number k_1 of the transmitted wave is obtained as a solution of the energy conservation relation

$$\epsilon(k_0) = -\epsilon(k_1) + \Phi_0 \equiv \epsilon_0, \tag{A17}$$

where $\epsilon(k)$ is defined by Eq. (6) given in the text. Note that the solution $k_1 < 0$ to Eq. (A17) must be chosen to ensure a positive group velocity of transmitted wave packet (progressive wave). The transmission coefficient T_D is then readily calculated as

$$T_D = 1 - \left|\frac{-k_1(\epsilon_0 - \delta) + k_0(\epsilon_0 - \delta - \Phi_0)}{k_1(\epsilon_0 - \delta) + k_0(\epsilon_0 - \delta - \Phi_0)}\right|^2. \tag{A18}$$

A comparison of the transmission coefficients T and T_D, given by Eqs. (7) and (A18), is discussed in the text with reference to Fig. 3.

[1] O. Klein, Z. Phys. **53**, 157 (1929).
[2] W. Greiner, *Relativistic Quantum Mechanics* (Springer-Verlag, Berlin, 1990), Chap. 13.
[3] A. Calogeracos and N. Dombey, Contemp. Phys. **40**, 313 (1999).
[4] H. Nitta, T. Kudo, and H. Minowa, Am. J. Phys. **67**, 966 (1999).
[5] F. Sauter, Z. Phys. **69**, 742 (1931).
[6] K. S. Novoselov, A. K. Geim, S. V. Morozov, D. Jiang, M. I. Katsnelson, I. V. Grigorieva, S. V. Dubonos, and A. A. Firsov, Nature (London) **438**, 197 (2005).
[7] S. Y. Zhou, G.-H. Gweon, J. Graf, A. V. Fedorov, C. D. Spataru, R. D. Diehl, Y. Kopelevich, D.-H. Lee, Steven G. Louie, and A. Lanzara, Nat. Phys. **2**, 595 (2006).
[8] M. I. Katsnelson, K. S. Novoselov, and A. K. Geim, Nat. Phys. **2**, 620 (2006).
[9] C. W. J. Beenakker, Rev. Mod. Phys. **80**, 1337 (2008).
[10] A. H. Castro Neto, F. Guinea, N. M. Peres, K. S. Novoselov, and A. K. Geim, Rev. Mod. Phys. **81**, 109 (2009).
[11] V. V. Cheianov and V. I. Fal'ko, Phys. Rev. B **74**, 041403(R) (2006); A. Ossipov, M. Titov, and C. W. J. Beenakker, *ibid.* **75**, 241401 (2007); C. Bai and X. Zhang, *ibid.* **76**, 075430 (2007); A. De Martino, L. Dell'Anna, and R. Egger, Phys. Rev. Lett. **98**, 066802 (2007); C. W. J. Beenakker, A. R. Akhmerov, P. Recher, and J. Tworzydło, Phys. Rev. B **77**, 075409 (2008); P. Hewageegana and V. Apalkov, *ibid.* **79**, 115418 (2009); E. Romera and F. de los Santos, *ibid.* **80**, 165416 (2009); Cs. Péterfalvi, A. Pályi, and J. Cserti, *ibid.* **80**, 075416 (2009).
[12] A. F. Young and P. Kim, Nat. Phys. **5**, 222 (2009).
[13] N. Stander, B. Huard, and D. Goldhaber-Gordon, Phys. Rev. Lett. **102**, 026807 (2009).
[14] G. A. Steele, G. Gotz, and L. P. Kouwenhoven, Nat. Nanotechnol. **4**, 363 (2009).
[15] F. D. M. Haldane and S. Raghu, Phys. Rev. Lett. **100**, 013904 (2008).
[16] R. A. Sepkhanov, Ya. B. Bazaliy, and C. W. J. Beenakker, Phys. Rev. A **75**, 063813 (2007).
[17] O. Peleg, G. Bartal, B. Freedman, O. Manela, M. Segev, and D. N. Christodoulides, Phys. Rev. Lett. **98**, 103901 (2007).
[18] O. Bahat-Treidel, O. Peleg, and M. Segev, Opt. Lett. **33**, 2251 (2008).
[19] X. Zhang, Phys. Rev. Lett. **100**, 113903 (2008).
[20] T. Ochiai and M. Onoda, Phys. Rev. B **80**, 155103 (2009).
[21] O. Bahat-Treidel, O. Peleg, M. Grobman, N. Shapira, T. Pereg-Barnea, and M. Segev, arXiv:0905.4278 (unpublished).
[22] D. Ö. Güney and D. A. Meyer, Phys. Rev. A **79**, 063834 (2009).
[23] F. Dreisow, A. Szameit, M. Heinrich, T. Pertsch, S. Nolte, A. Tünnermann, and S. Longhi, Phys. Rev. Lett. **102**, 076802 (2009).
[24] S. Longhi, Laser Photonics Rev. **3**, 243 (2009).
[25] A. A. Sukhorukov and Y. S. Kivshar, Opt. Lett. **27**, 2112 (2002).
[26] S. Longhi, Opt. Lett. **31**, 1857 (2006).
[27] A. A. Sukhorukov, D. Neshev, W. Krolikowski, and Y. S. Kivshar, Phys. Rev. Lett. **92**, 093901 (2004).
[28] S. Longhi, M. Lobino, M. Marangoni, R. Ramponi, P. Laporta, E. Cianci, and V. Foglietti, Phys. Rev. B **74**, 155116 (2006).
[29] S. Longhi, Opt. Lett. **35**, 235 (2010).
[30] Note that for a beam incident onto the array at an angle θ close to, but distinct than, the Bragg angle θ_B, we can still write $E(x,0)=G(x)\exp(2\pi i\theta_B n_s x/\lambda)$, the mismatch between θ and θ_B being included in a phase term $\sim\exp[2\pi i(\theta-\theta_B)n_s x/\lambda]$ of the envelope $G(x)$.
[31] S. Suntsov, K. G. Makris, D. N. Christodoulides, G. I. Stegeman, R. Morandotti, M. Volatier, V. Aimez, R. Arè, C. E. Rüter, and D. Kip, Opt. Express **15**, 4663 (2007); M. I. Molina and Y. S. Kivshar, Phys. Lett. A **362**, 280 (2007); A. Szameit, H. Trompeter, M. Heinrich, F. Dreisow, U. Peschel, T. Pertsch, S. Nolte, F. Lederer, and A. Tünnermann, New J. Phys. **10**, 103020 (2008).
[32] Precisely, the wave-packet dynamics of our optical system reproduces the case of Fig. 3 of Ref. 4, rather than the case of Fig. 4 of the same reference, where electron-positron pairs creation at the potential step is assumed, resulting in a reflected current larger than the incident one. This effect is sometimes referred to as the Klein paradox. The issue of electron-positron pairs creation for a potential step and its consequences, however, has been a matter of a great debate [see, for instance,[3] and the discussions in: S. Danko Bosanac, J. Phys. A **40**, 8991 (2007); D. Dragoman, Phys. Scr. **79**, 015003 (2009)].
[33] P. Christillin and E. d'Emilio, Phys. Rev. A **76**, 042104 (2007).
[34] S. Nolte, M. Will, J. Burghoff, and A. Tünnermann, Appl. Phys. A: Mater. Sci. Process. **77**, 109 (2003); K. Itoh, W. Watanabe, S. Nolte, and C. Schaffer, MRS Bull. **31**, 620 (2006).
[35] R. Khomeriki, Phys. Rev. Lett. **92**, 063905 (2004).
[36] J. Viana Gomes and N. M. R. Peres, J. Phys.: Condens. Matter **20**, 325221 (2008).